Coupling induced emergent topology in a two-leg fermionic ladder

Rajashri Parida[1,2], Biswajit Paul[1,2] , Soumya Ranjan Padhi[1,2] and Tapan Mishra[1,2*]

[1] *School of Physical Sciences, National Institute of Science Education and Research, Jatni, Odisha 752050, India*
[2] *Homi Bhabha National Institute, Training School Complex, Anushaktinagar, Mumbai, Maharashtra 400094, India*

(Dated: October 8, 2025)

We investigate the ground state properties of spinless fermions on a two leg ladder, by allowing the nearest-neighbour hopping dimerization in one leg and uniform hopping in the other. In the non-interacting limit, we find that, at half-filling, the system exhibits robust topological behavior if the inter-leg hopping is allowed. Though depending on the dimerization pattern, the dimerized leg can be either topological or trivial in nature, here we show that by connecting such a leg to a uniform leg through inter-chain coupling, the overall system becomes topological irrespective of the dimerization pattern in the dimerized leg. As a result, a topological phase transition occurs as a function of the inter-leg hopping. When the inter-leg interaction is turned on, the topological phase survives, and we obtain an interaction induced topological phase transition. Finally, we reveal that when uniform interactions are included on all the bonds of the ladder, the topological phase transitions to a symmetry-broken charge-density wave (CDW) phase.

I. INTRODUCTION

Over the past decades, the notion of topology has emerged as a powerful framework for understanding novel quantum phases of matter that fall beyond the conventional Landau symmetry-breaking paradigm [1]. Unlike conventional phases classified by local order parameters and spontaneous symmetry breaking, topological phases are characterized by global, quantized invariants associated with the wavefunctions of the system. Band topology, in particular, has reshaped the classification of insulating phases in non-interacting systems, giving rise to robust edge or surface states protected by underlying symmetries [2]. One such example is the symmetry-protected topological (SPT) phase, which possesses robust boundary states as long as certain symmetries are preserved. The celebrated model that exhibits band topology and an SPT phase is the Su-Schrieffer-Heeger (SSH) model of non-interacting fermions [3], which hosts topologically protected edge states arising from the dimerized hopping in a one-dimensional chain. The SSH model, due to its simplicity, has been extensively studied [4–8], and its topological features have been realized in diverse experimental platforms, including cold atoms, photonic and acoustic lattices, superconducting and electrical circuits, ion traps, and mechanical systems [9–25].

These ideas have now expanded beyond non-interacting limits, opening new avenues for exploring how strong correlations, dimensionality, and symmetry intertwine to stabilize or destabilize topological order in the free fermionic counterpart [26]. In this context, SPT serves as the simplest playground to study the interplay of these key aspects of quantum condensed matter physics, as these phases are short-range entangled phases [27, 28]. Due to this, extensive research has been conducted using interacting SSH models to understand how local and non-local interactions affect topological phases and phase transitions in many-body fermionic, bosonic, and spin systems [29–41]. An interesting revelation in this context is the interaction induced topology where interactions alone give rise to nontrivial topology in systems that are otherwise topologically trivial in the non-interacting limit [42–47].

On the other hand, interaction effects and dimensionality of the lattices on the topological phases have been investigated by going beyond strictly one-dimensional chains. In particular, ladder geometries or quasi-one dimensional lattices that are intermediate to one and two-dimensional lattices have attracted a great deal of attention, revealing interesting topological properties [33, 48–63]. The key component in the ladder systems that plays the major role is the inter-layer coupling that decides the fate of the topological properties of individual chains and may impart novel physical phenomena due to proximity effects [64–68].

In this work, we study the topological properties of an asymmetric two-leg ladder model composed of spinless fermions, where one leg follows the SSH-type dimerized hopping, and the other is a uniform tight-binding chain. For the non-interacting case, the dimerization pattern decides the topological or trivial nature of the SSH-type leg. However, once coupled to a uniform tight-binding chain through interchain tunneling, the ladder as a whole becomes topological regardless of the dimerization pattern in the dimerized leg. Interestingly, in the many-body limit, including the rung interaction, it also drives a topological phase transition in the system as a function of rung interaction. However, when uniform interactions are introduced along both the legs and rungs, this topological phase transition ceases to happen, and the system instead undergoes a transition into a CDW phase.

The paper is organized as follows. In sec. II, we in-

* mishratapan@gmail.com

troduce the model under consideration and the computational method used to obtain all the results. In sec. III A, we present the non-interacting case, focusing on both regimes of dimerization in the SSH-type leg. Sec. III B discusses the scenario when interaction between the particles is considered. Finally, in sec. IV, we provide a summary of the key results.

II. MODEL

We consider a system of spinless fermions on a two-leg ladder depicted in Fig. 1, where uniform and SSH type dimerized hopping patterns in the lower and the upper legs have been assumed, respectively. The model that describes such a system is given by the Hamiltonian,

$$\hat{H}_M = \hat{H} + \hat{H}_{V_p} \tag{1}$$

where,

$$\hat{H} = -\Bigg(\sum_{i\in\text{odd}} t_1 \hat{a}_i^\dagger \hat{a}_{i+1} + \sum_{i\in\text{even}} t_2 \hat{a}_i^\dagger \hat{a}_{i+1} + t \sum_i \hat{b}_i^\dagger \hat{b}_{i+1} + t_p \sum_i \hat{a}_i^\dagger \hat{b}_i \Bigg) + \text{H.c.} \tag{2}$$

$\hat{H}$ represents the Hamiltonian of non-interacting spinless fermions. $\hat{a}_i(\hat{a}_i^\dagger)$ and $\hat{b}_i(\hat{b}_i^\dagger)$ are the particle annihilation (creation) operators on leg-a and leg-b, respectively, where i represents the rung index. t_1 and t_2 are the alternating hopping amplitudes in the upper leg, t is the uniform hopping strength in the lower leg, and t_p represents the strength of the rung (inter-leg) hopping. Throughout all the numerical calculations, we set $t = 1$, which sets the energy scale of the system.

Since the single-particle Hamiltonian $\hat{H}$ has a unit cell consisting of four lattice sites, Fourier transforming the Hamiltonian in Eq. (2) yields

$$\hat{H}_k = \begin{bmatrix} 0 & \mu_1 & 0 & -t_p \\ \mu_1^* & 0 & -t_p & 0 \\ 0 & -t_p & 0 & \mu_2 \\ -t_p & 0 & \mu_2^* & 0 \end{bmatrix} \tag{3}$$

where we have set the lattice constant to unity, $\mu_1 = -t_1 - t_2 e^{-ik}$ and $\mu_2 = -t(1 + e^{ik})$, with k representing the quasi-momentum.

In terms of Pauli matrices, the above Hamiltonian can be written as

$$\begin{aligned} \hat{H}_k &= -\{[(t_1 + t) + (t_2 + t)\cos(k)]\sigma_x \\ &+ (t_2 - t)\sin(k)\sigma_y\} \otimes \frac{\mathbf{I}}{2} \\ &- \{[(t_1 - t) + (t_2 - t)\cos(k)]\sigma_x \\ &+ (t_2 + t)\sin(k)\sigma_y\} \otimes \frac{\nu_z}{2} - t_p\sigma_x \otimes \nu_x \end{aligned} \tag{4}$$

where ν_m's and σ_m's with $m = (x,\ y,\ z)$, are the Pauli matrices corresponding to the leg of the ladder and sublattice in each leg. $\mathbf{I}$ represents the 2×2 identity matrix.

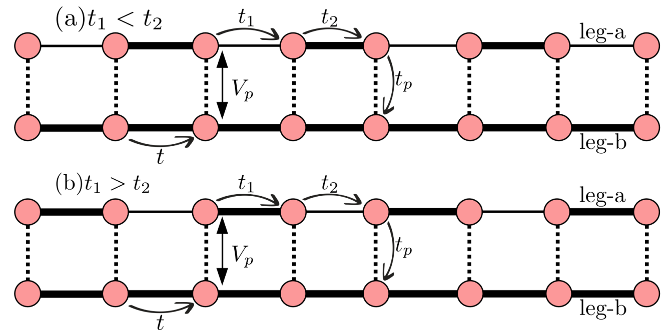

FIG. 1. Schematic of a two-leg ladder with dimerized hopping along the upper leg. The circles denote lattice sites. The alternating hopping amplitudes are t_1 and t_2, where the stronger hopping is represented by thick solid lines and the weaker hopping by thin solid lines. The lower leg has uniform hopping, shown by thick solid lines. Panel (a) corresponds to $t_1 < t_2$, while panel (b) corresponds to $t_1 > t_2$.

Upon introducing interactions between the fermions, the above model exhibits characteristics of a strongly correlated Fermi system. For simplicity, we consider only rung-wise repulsive interactions, which can be incorporated as the term $\hat{H}_{V_p}$ in Eq. (1)

$$\hat{H}_{V_p} = V_p \sum_i (\hat{n}_{i,a} - \frac{1}{2})(\hat{n}_{i,b} - \frac{1}{2}), \tag{5}$$

where $\hat{n}_{i,a}$ ($\hat{n}_{i,b}$) represents the occupation density in the upper (lower) leg of the ladder.

We investigate the many-body ground state properties of the system using the matrix product state (MPS) version of the density matrix renormalization group (DMRG) method [69, 70] under open boundary conditions (OBC). For specific cases, we complement our analysis with exact diagonalization (ED) using periodic boundary conditions (PBC). In the DMRG calculations, the system size is taken up to $L = 200$ rungs ($= 400$ sites), with a maximum bond dimension of 800 to minimize truncation errors. A system of size $L = 12$ rungs (24 sites) is used for ED simulations. Unless otherwise mentioned, all observables are extrapolated to the thermodynamic limit.

III. RESULTS

In this section, we first analyze the noninteracting case, where we investigate the effect of rung hopping, and then we investigate the role of interparticle interaction.

A. Non-interacting case

To understand the topological nature of the non-interacting particles, we begin by examining the gap-opening as well as the gap-closing scenarios. Since in

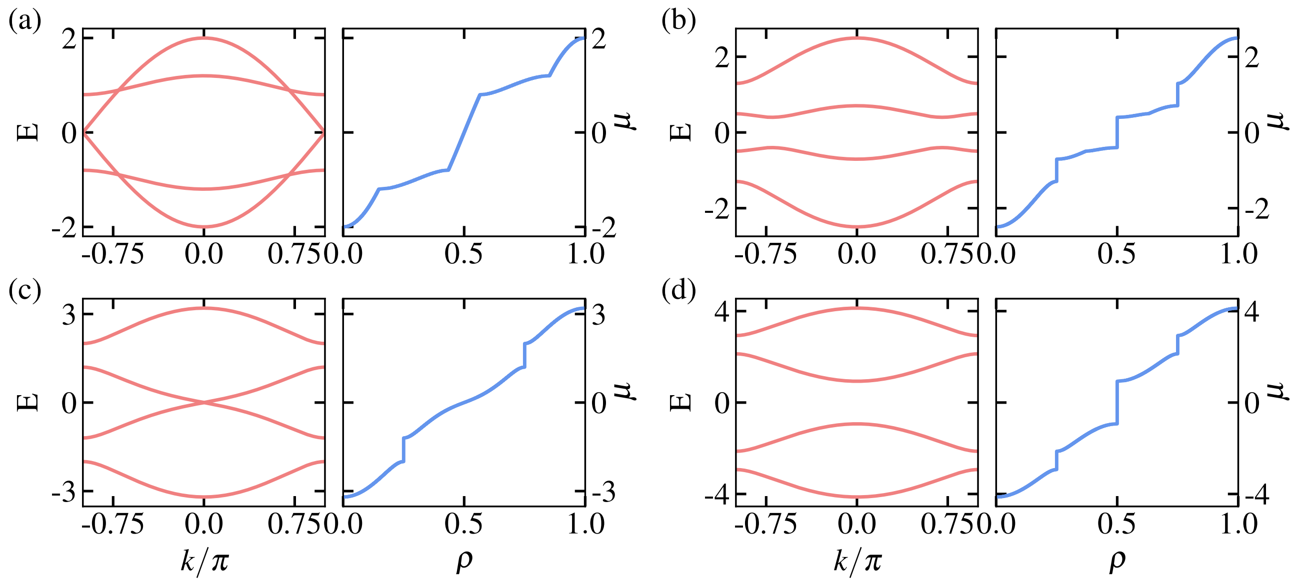

FIG. 2. The left panels in (a-d) represent the single particle dispersion bands for $t_p = 0.0,\ 0.8,\ \sqrt{2.4},$ and 2.5 respectively. The right panels in (a-d) represent the corresponding particle filling (ρ) plotted against the chemical potential (μ) for the same values of t_p with a system of $L = 500$ rungs. For all the plots, the values of t_1 and t_2 are fixed at 0.2 and 1.0 respectively.

fermionic systems, the energy gaps can be fully understood from the underlying band structure, we start by diagonalizing the Hamiltonian given in Eq. (4), and the resulting dispersion relation is

$$E^2 = t_p^2 + \frac{1}{2}(|\mu_1|^2 + |\mu_2|^2) \pm \frac{1}{2}\sqrt{(2t_p^2 + |\mu_1|^2 + |\mu_2|^2)^2 + 4(\mu_1\mu_2 - t_p^2)(t_p^2 - \mu_1^*\mu_2^*)}, \tag{6}$$

where, μ_1 and μ_2 are as defined earlier.

The above dispersion relation suggests that for any finite dimerization in hopping in leg-a, the gap closes at $k = 0$ when $t_p^2 = 2t(t_1 + t_2)$, and at $k = \pi$, when $t_p^2 = 0$. At all other points, the gap remains open at half-filling. We display the band structure for four exemplary values of t_p: $t_p = 0,\ 0.8,\ \sqrt{2.4}$, and 2.5 in the left panles of Fig. 2(a–d) respectively by fixing $t_1 = 0.2$ and $t_2 = 1.0$. To compare the band picture with the filling of particles in real space, the filling $\rho = N/2L$ as a function of chemical potential μ [71] calculated under PBC, is plotted in right panels of Fig. 2(a–d), where N is the total number of fermions and L is the number of rungs. The appearance of cusps in the ρ–μ curves reflects changes in the number of Fermi points i.e., the number of quasi-momenta where the Fermi energy intersects the bands. The width of each plateau in the ρ–μ curve indicates the value of the energy gap at the corresponding filling, whereas the shoulder regions around the plateaus indicate the gapless Luttinger liquid. Comparing the two panels in Fig. 2(a), we observe that for $t_p = 0$, the system remains gapless at all fillings. In contrast, for $t_p = 0.8$, finite gaps emerge at $\rho = 1/4,\ 1/2,$ and $3/4$, as shown in Fig. 2(b). Increasing the value of t_p to $\sqrt{2.4}$ closes the gap at $\rho = 1/2$, while the gaps at $\rho = 1/4,$ and $3/4$ persist [see Fig. 2(c)]. At $t_p = 2.5$, gaps reappear again at all three commensurate fillings, such as for $\rho = 1/4,\ 1/2,$ and $3/4$, as shown in Fig. 2(d).

With this information in hand about the gap of the system, we investigate topological phase transitions in the subsequent subsection.

1. *Topological Phase Transition*

Since one of the legs of the ladder is considered to be of SSH type, we can have two possible dimerization patterns: (i) topological pattern ($t_1 < t_2$ as in Fig. 1(a)) and (ii) the trivial pattern ($t_1 > t_2$ as in Fig. 1(b)). For the topological (trivial) pattern, we choose $t_1 = 0.2,\ t_2 = 1.0$ ($t_2 = 1.0,\ t_2 = 0.2$). Note that the hopping in the other leg is uniform throughout and is set to $t = 1.0$. This choice of hopping suggests that in the decoupled leg limit, the leg-a can be either trivial or a topological insulator whereas the leg-b is always a gapless Luttinger liquid. Our goal is to investigate the influence of the dimerized leg on the system when the two legs are coupled to each other. We first explore the real space energy spectrum of the system under OBC. In Fig. 3(a) and (b) we depict the energy spectrum as a function of t_p for $t_1 < t_2$ and $t_1 > t_2$ configurations, respectively. For both the configurations, the bulk gaps open up as soon as t_p becomes finite. Interestingly, for both the topological and trivial dimerization configuration of leg-a, the bulk gap hosts two mid-gap zero-energy states which disappear at a crit-

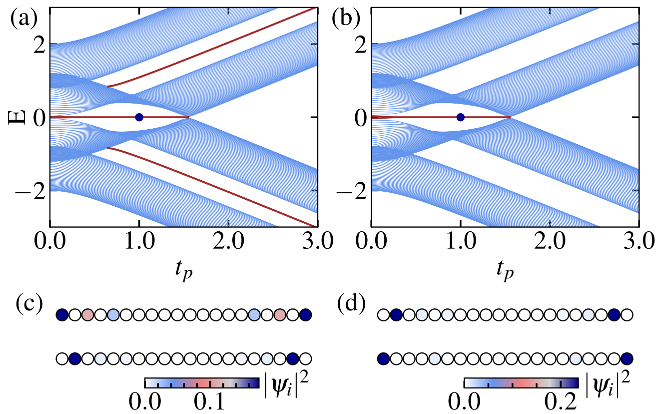

FIG. 3. (a) and (b) energy spectrum as a function of rung hopping t_p when $t_1 = 0.2$, $t_2 = 1.0$ and $t_1 = 1.0$, $t_2 = 0.2$ respectively. (c) and (d) represent the probability density $|\psi_i|^2$, where the circles represent the sites of the ladder and the facecolor of the circle represents the probability density corresponding to the blue circle in (a) and (b), respectively.

ical $t_p = \sqrt{2.4}$ with the closing up of the bulk gap. However, the gap reopens with further increase in t_p without the zero energy states. These zero energy states are typical signatures of topological phases under OBC. In order to examine that these zero-energy states are edge states, we plot the onsite probability density ($|\psi_i|^2$) corresponding to one of these two states. As shown in Fig. 3(c) and (d) the states corresponding to the dimerization patterns $t_1 = 0.2$, $t_2 = 1.0$ and $t_1 = 1.0$, $t_2 = 0.2$ for an exemplary value $t_p = 1.0$ (dots in Fig. 3(a) and (b)), are localized at the edges of the system. The key distinction between both the cases is that the edge states exist on the upper leg when $t_1 < t_2$ and on the lower leg when $t_1 > t_2$. Interestingly, we observe the lower-leg, which doesn't have any hopping dimarization, has supported a zero energy edge state. Additionally, the spectra also exhibit isolated energetic mid-gap states at $\rho = 1/4$ and $\rho = 3/4$ fillings for $t_1 < t_2$ (the red solid lines), which are absent for $t_1 > t_2$. For $\rho = 1/2$, it is evident that there is a pair of localized edge modes existing in the upper leg for the $t_1 < t_2$ case, whereas at $\rho = 1/4$, the edges of both the legs of the ladder hybridize (not shown), resulting in energetic edge states. In contrast, there is also another pair of edge modes at zero energy for $t_1 > t_2$ case as shown in Fig. 3(d), and these are localized in the lower leg of the ladder. From now on, we focus on the zero energy edge states appearing at half-filling to characterize the topological property of our system, as these are the states protected by symmetry.

To concretely establish this topological feature, we compute the topological invariant called the Berry phase (ω) [72], which is defined as

$$\omega = -\Im \ \ln \prod_{j=0}^{N-1} \det(\langle u_{m,k_j} | u_{n,k_{j+1}} \rangle), \tag{7}$$

where, $\Im$ denotes the imaginary part, $k_j = 2\pi j/Na$ is the j^{th} k point in the Brillouin zone and $|u_{m,k_j}\rangle$ denotes the occupied Bloch bands with m and n representing the band indices. The determinant is taken as we are dealing with a multiband system. It is well known that a trivial bulk is characterized by $\omega = 0$, while a topological bulk possesses a value $\omega = \pi$. We calculate the Berry phase ω for both $t_1 < t_2$ as well as $t_1 > t_2$ cases by taking the filled bands up to half filling and plot ω/π, called the winding number, as a function of t_p in Fig. 4(a) and (b), respectively. At $t_p = 0$, the two legs of the ladder are completely decoupled, with one forming a tight-binding chain for which the gap closes at $k = \pi$, making the Berry phase undefined. For any finite t_p, however, the system acquires a well-defined Berry phase, which takes the value π for both $t_1 < t_2$ and $t_1 > t_2$ for arbitrarily small t_p, confirming the topological nature of the phases. As t_p increases, the bulk gap closes at $t_p = \sqrt{2.4}$, beyond which the Berry phase drops to 0, indicating a transition to a trivial phase. This change in ω/π from 1 to 0 for both $t_1 < t_2$ and $t_1 > t_2$ provides clear evidence of a topological phase transition at $t_p = \sqrt{2.4}$. Furthermore, this transition is also accompanied by the disappearance of the zero-energy edge modes present in the topological phase, and this is called the bulk-boundary correspondence in our system.

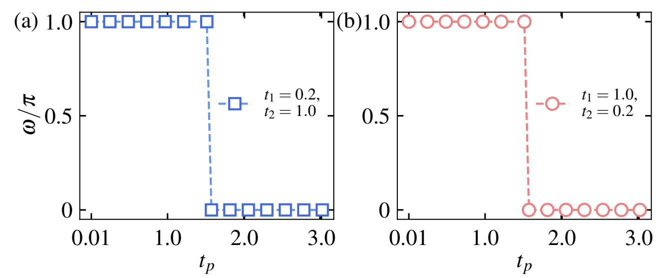

FIG. 4. (a) and (b) illustrate winding number as a function of t_p when $t_1 = 0.2$, $t_2 = 1.0$ and $t_1 = 1.0$, $t_2 = 0.2$, respectively.

2. Phase diagram

Based on the above analysis of the appearance of zero-energy edge modes under OBC and the quantized topological invariant ω under PBC, we now demonstrate the topological phase transitions in the form of phase diagrams. For this purpose, we characterize the topological properties of the system as a function of t_p for different values of dimerization strength, that is by fixing $t_2 = 1.0$ and varying t_1. To this end, we compute the energy gap (G), defined as the energy difference between the two eigenstates at the middle of the bulk gap (i.e., at $\rho = 1/2$), and is given by $G = E_L - E_{L-1}$ under OBC. The plot of G (color coded) as a function of t_p and t_1 while fixing $t_2 = 1.0$ is shown in Fig. 5(a). The blue regions, where G vanishes, indicate the presence of degen-

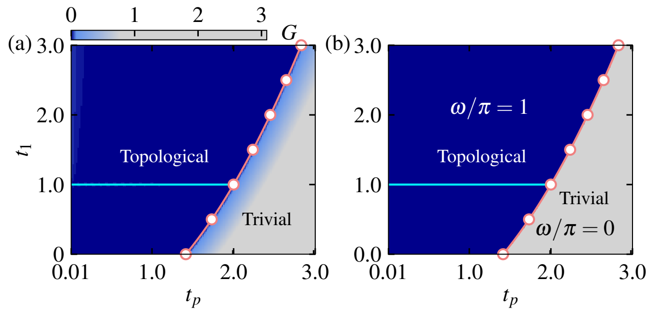

FIG. 5. The phase diagram in the $t_p - t_1$ plane is shown for $t_2 = 1.0$. In panel (a), the color bar represents the single-particle excitation gap (G) at half-filling, computed for a system of size $L = 480$ under OBC. In panel (b), the blue regions correspond to a winding number $\omega/\pi = 1$ and gray regions to $\omega/\pi = 0$ obtained under PBC. The horizontal lines at $t_1 = t_2 = 1.0$ indicate the gapless line.

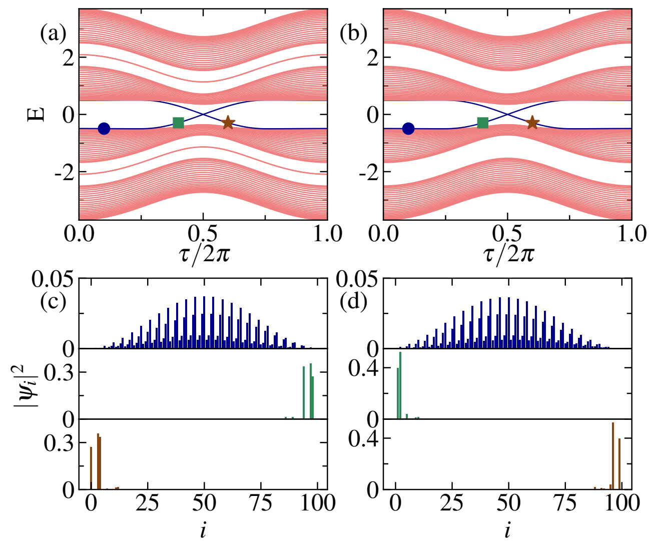

FIG. 6. Instantaneous energy spectrum of the Hamiltonian $\hat{H}_p$ as a function of the pumping parameter τ, computed for a system of $L = 50$ rungs under OBC. Panel (a) corresponds to the parameter set $t_1 = 0.2$, $t_2 = 1.0$, while panel (b) shows results for $t_1 = 1.0$, $t_2 = 0.2$. In both cases, the pumping parameters are fixed at $t_{p_0} = 1.55$, $\delta_0 = 0.5$, and $\Delta_0 = 0.5$. The highlighted markers in (a) and (b) blue circle, green square, and brown star, indicate specific states whose probability amplitudes are shown in panels (c) and (d), respectively. In panel (c), the top, middle, and bottom subplots show the probability density $|\psi_i|^2$ plotted against the site index for the states marked in (a). Analogously, panel (d) presents the probability density corresponding to the marked states in (b).

erate zero-energy modes at $\rho = 1/2$, whereas in the gray region, G acquires finite values due to the absence of any degenerate edge states. For a fixed t_1, G remains zero up to a critical value of t_p, beyond which it becomes finite, suggesting a topological phase transition. The point at which this topological phase transition occurs agrees well with the analytical boundary at $t_p = \sqrt{2t(t_1 + t_2)}$ (indicated by the red line with circles). Note that at $t_1 = t_2$, the entire bulk is gapless up to $t_p \leq 2$ indicated by the horizontal solid line in Fig. 5(a). In Fig. 5(b) we plot the bulk topological invariant ω/π (the winding number) defined in Eq. (14) for the same parameters as in Fig. 5(a). The values of $\omega/\pi = 1$ (0) confirms the topological (trivial) regions. This clearly complements the topological to trivial phase transition as a function of t_p. Note that in the gapless region at $t_1 = t_2 = 1.0$ and up to $t_p \leq 2$, the invariant is ill-defined due to the absence of a bulk energy gap and hence the value is not fixed in these parameter regimes.

The above analysis demonstrates that a well-defined topological phase emerges in the system due to t_p, regardless of the dimerization pattern in leg-a, i.e., whether $t_1 < t_2$ or $t_1 > t_2$. Moreover, an increase in the value of t_p favours a topological to trivial phase transition for any fixed dimerization strength. In the following, we will quantify the above topological phase transition occurring at $\rho = 1/2$ through a quantity that serves as a dynamic probe for characterizing the above topological phase transitions, and also highlight the phenomenon of reversal of Thouless charge pumping.

3. *Reversal of Thouless charge pumping*

Thouless charge pumping (TCP) [73] is a versatile platform to characterize the topological phase in the system through periodic modulation of system parameters. This involves slow and cyclic variation of at least two parameters in the system resulting in a quantized particle transport even in the absence of an external bias. One of the parameters drives the system through a topological phase transition, while an additional staggered potential term breaks the inversion symmetry and maintains a finite bulk gap throughout the cycle. This is crucial for ensuring adiabaticity, which is a key requirement for quantized charge transport. During the adiabatic cycle, the system traverses from a topological phase to a trivial phase and back to the initial topological phase, enclosing the topological phase transition point. This process results in the transport of a quantized number of particles and, the number of particles transported is solely determined by the topological invariant, i.e., the Chern number of the system. TCP has been widely investigated in various theoretical and experimental studies in recent years as a key tool for understanding topological phase transitions [10, 11, 34, 52, 74–92]. The Rice-Mele model provides a well-established framework for describing charge pumping protocols. To investigate the topological phase transition occurring as a function of t_p at $\rho = 1/2$, we propose a pumping protocol that is governed

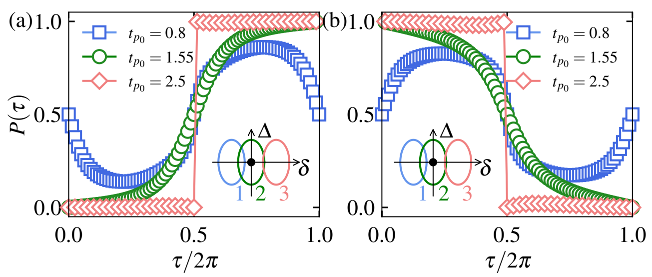

FIG. 7. Evolution of polarization $P(\tau)$ as a function of τ for (a) $t_1 = 0.2, t_2 = 1.0$ and (b) $t_1 = 1.0, t_2 = 0.2$. The plot shows results for three pumping cycles with different values of t_{p_0} ($= 0.8, 1.55, 2.5$), as indicated in the inset. In all cases, $\delta_0 = 0.5$ and $\Delta_0 = 0.5$. The polarization changes are represented by blue squares (cycle 1), green circles (cycle 2), and red diamonds (cycle 3).

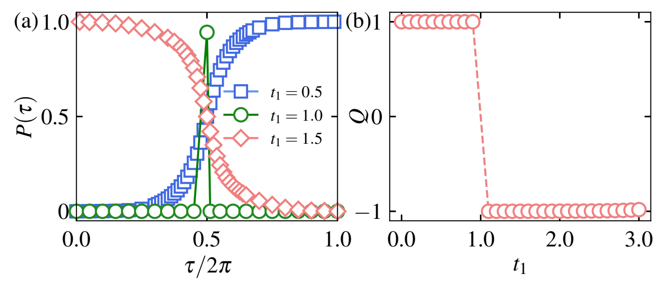

FIG. 8. (a)The evolution of polarization ($P(\tau)$) as a function of τ at $t_{p_0} = 2$ for three different values of t_1 i.e., 0.5 (blue squares), 1.0 (green circles), and 1.5 (red diamonds), keeping $t_2 = 1$ (Refer Phase diagram shown in Fig. 5). The pumping parameters are set to be $t_{p_0} = 2.0, \delta_0 = 1.0$ and, $\Delta_0 = 0.6$ (b) The amount of charge pumped (Q) by varying t_1 with fixed value of $t_{p_0} = 2.0$.

by the Hamiltonian

$$\begin{aligned}\hat{H}_p = &-\Bigg(\sum_{i\in\text{odd}} t_1 \hat{a}_i^\dagger \hat{a}_{i+1} + \sum_{i\in\text{even}} t_2 \hat{a}_i^\dagger \hat{a}_{i+1} + t \sum_i \hat{b}_i^\dagger \hat{b}_{i+1} \\ &+ (t_{p_0} + \delta(\tau)) \sum_i \hat{a}_i^\dagger \hat{b}_i \Bigg) + \text{H.c.} \\ &+ \sum_i \Delta(\tau)((-1)^{i+1} \hat{a}_i^\dagger \hat{a}_i + (-1)^i \hat{b}_i^\dagger \hat{b}_i). \end{aligned} \tag{8}$$

Here, τ is the pumping parameter and Δ ensures that the bulk gap remains open throughout the cycle. $(t_{p_0}, 0)$ is the origin of the pumping cycle in the $\delta-\Delta$ plane. $\delta(\tau) = \delta_0\cos(\tau)$ and $\Delta(\tau) = \Delta_0\sin(\tau)$ periodically modulate the rung hopping strength (t_p) and the staggered potential term, respectively.

To investigate the charge pumping mechanism, we present the instantaneous energy spectrum of the Hamiltonian defined in Eq. (8) for a system of size $L = 100$ rungs under OBC. Fig. 6(a) and (b) show the spectra for $t_1 < t_2$ and $t_1 > t_2$, respectively. The cyclic variation of the pumping parameters is represented by cycle-2 (highlighted by a green circle in the insets of Fig. 7(a) and (b)), which encloses the topological phase transition point. In both cases, at $\rho = 1/2$, two in-gap modes cross during the cycle, one ascending from the lower to the upper band and the other descending in the opposite direction after a certain value of the pumping parameter. To demonstrate their edge nature and the evolution during the pump, we plot the probability density of these modes just before and after the half-cycle (i.e. $\tau/2\pi = 0.5$), which correspond to the green square and brown star marked points in Figs. 6(a) and (b), respectively. The probability amplitudes are shown in the middle and lower panels of Figs. 6(c) and (d), respectively. These plots confirm that these modes exchange their position from one edge to another edge across the cycle, realizing topological pumping from one edge site to another edge site of the chain. For $t_1 < t_2$, the edge mode initially localized at the right end of the chain moves to the left after $\tau/2\pi = 0.5$, and vice versa for $t_1 > t_2$. This clearly illustrates the reversal of the topological charge pumping direction, governed by the relative dimerization pattern of t_1 and t_2. Since the cycle starts from a trivial phase, initially all states near half-filling have finite probability in the bulk, which is shown in the upper panels of Fig. 6(c) and (d) corresponding to the blue circle in Fig. 6(a) and (b), respectively.

To complement the reversal of the charge pumping phenomenon, we compute the electronic polarization P using the occupied Bloch bands of the Rice-Mele Hamiltonian under PBC as

$$P = -\frac{1}{2\pi}\Im\ \ln \prod_{j=0}^{N-1} \det(\langle u_{m,k_j} | u_{n,k_{j+1}} \rangle) \ (\text{mod } Qa), \tag{9}$$

where $|u_{m,k_j}\rangle$ denotes the occupied Bloch bands of the Hamiltonian

$$H_k = \begin{bmatrix} \Delta(\tau) & \mu_1 & 0 & -t_p - \delta(\tau) \\ \mu_1^* & -\Delta(\tau) & -t_p - \delta(\tau) & 0 \\ 0 & -t_p - \delta(\tau) & \Delta(\tau) & \mu_2 \\ -t_p - \delta(\tau) & 0 & \mu_2^* & -\Delta(\tau) \end{bmatrix}. \tag{10}$$

Here, Q denotes the particle charge and a is the lattice constant (set to unity). We calculate the value of P at different values of τ, which we call $P(\tau)$ and the amount of charge pumped in a cycle is given by

$$Q = \int_0^{2\pi} d\tau\ \partial_\tau P(\tau). \tag{11}$$

It is evident from Fig. 7(a) that only the cycle 2 results in a smooth variation of $P(\tau)$ from 0 to 1, corresponding to a quantized charge transfer of $Q = +1$. For the cycle-1, no pumping occurs, while the cycle-3 shows discontinuity in $P(\tau)$, indicating a breakdown of transport. We further explore the scenario by switching the dimerization to $t_1 = 1.0$, $t_2 = 0.2$, while keeping other parameters fixed. In this case, $P(\tau)$ evolves from 1 to 0 for cycle-2, implying a reversed pumping direction with $Q = -1$ [see Fig. 7(b)]. This confirms that the direction of charge transport depends on the dimerization pattern, and altering the dimerization pattern reverses the direction of pumping. To further illustrate the reversal of charge pumping, we fix the rung hopping to $t_p = 2$ in the phase diagram [Fig. 5], and examine the evolution of polarization $P(\tau)$ for three different values of t_1: 0.5, 1.0, and 1.5, while keeping $t_2 = 1$ fixed [Fig. 8(a)]. For $t_1 = 0.5$ ($t_1 < t_2$), the polarization smoothly changes from 0 to 1 over the cycle, indicating a pumped charge of $Q = +1$. At $t_1 = 1.0$, the pumping path intersects the gap-closing point, leading to a breakdown of adiabatic transport and resulting in no net pumping. In contrast, for $t_1 = 1.5$ ($t_1 > t_2$), the polarization evolves from 1 to 0, corresponding to a pumped charge of $Q = -1$, demonstrating a reversal in the direction of charge transport compared to the $t_1 < t_2$ case. To quantify this reversal more generally, we compute the total pumped charge Q as a function of t_1, keeping all other parameters fixed as in Fig. 8(a). The resulting behavior, shown in Fig. 8(b), clearly shows that the amount of charge pumped changes from 1 to -1 as soon as one crosses the $t_1 = t_2$ point. This behavior captures the transition from positive to negative charge pumping, confirming the reversal of the charge pumping. From the above analysis, it is clear that we find the phenomenon of reversal of Thouless charge pumping by periodic modulation of the rung hopping strength. This phenomenon of reversal of TCP also indicates that the phases for $t_1 < t_2$ and $t_1 > t_2$ are topologically distinct.

Note that such topological phases do not exist for hard-core bosonic ladder, and it is solely due to fermionic statistics.

B. Interacting case

We now investigate how this topological phase arising in the non-interacting limit evolves upon introducing interactions in the system. We first explore the effect of inter-chain (rung) repulsive interactions V_p and then the effect of repulsive interactions along all the bonds of the system.

1. Effect of inter-chain interaction

Before analyzing the evolution of topological properties, we first present the bulk phase diagram in the $V_p - \mu$ plane, with $t_1 = 0.2,\ t_2 = 1.0$ and $t_p = 0.8$, which is depicted in Fig. 9. The white regions are the gapped phases, and the shaded regions are the gapless phases. The black dashed lines are the edge states, which are extracted by tracking the vanishing up of the single-particle excitation gap defined as $G = \mu_1^+ - \mu_1^-$, where

$$\mu_1^+ = E_{N+1} - E_N \quad \text{and} \quad \mu_1^- = E_N - E_{N-1}. \qquad (12)$$

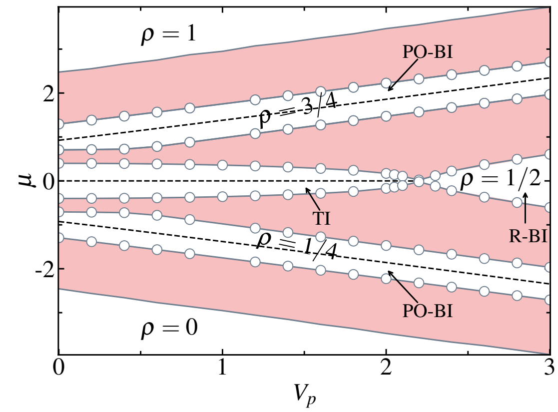

FIG. 9. The phase diagram in the $V_p - \mu$ plane keeping $t_1 = 0.2,\ t_2 = 1.0,\ t_p = 0.8$ fixed. Dashed lines represent the edge states. All the phase boundaries are extrapolated by taking a maximum system of size $L = 100$ rungs.

The boundaries of the gapped phases (gray solid lines with circles) are identified from the ρ - μ plots [93–95] for different values of V_p. Some exemplary behaviour of ρ as a function of μ are shown in Fig. 10.

In the $\rho - \mu$ curve, the appearance of plateaus indicates a gap, with the plateau width giving its magnitude. The lower and the upper phase boundaries shown in Fig. 9 are determined from the chemical potential values at the left and right ends of these plateaus in Fig. 10. All the phase boundaries obtained are extrapolated to the thermodynamic limit. It is evident from the phase diagram that there are three gapped phases, at $\rho = 1/4$, $1/2$ and $3/4$ fillings. The upper (lower) white region is the full (vacuum) state with $\rho = 1$ ($\rho = 0$).

To gain further insight into the nature of these gapped phases, we analyze the many-body ground state by examining the magnitude of the NN bond energies and onsite particle densities at different fillings $\rho = 1/4, 1/2,$ and $3/4$, as shown in the phase diagram in Fig. 9. To do this, we compute the bond energies on the legs ($B_{i,\alpha}$) and rungs ($B_{i,r}$) using the following expressions:

$$B_{i,\alpha} = \langle \hat{\alpha}_i^\dagger \hat{\alpha}_{i+1} + \text{H.c.} \rangle, \quad B_{i,r} = \langle \hat{a}_i^\dagger \hat{b}_i + \text{H.c.} \rangle \qquad (13)$$

where $\alpha = a, b$ denotes the legs, and r denotes the rungs. In Fig. 11, the bond thickness represents the magnitude of the bond energy, while the face color indicates the onsite particle density. The results are obtained for a system of $L = 100$ rungs at $V_p = 0.2$, 1.4, and 2.8, and the figure focuses only on the central 10 rungs to highlight the bulk behavior. At $\rho = 1/2$, Fig. 11(a) ($V_p = 0.2$) shows strong dimerization along the legs, with alternating bond strengths indicating a bond-ordered (BO) phase. In contrast, Fig. 11(b) reveals stronger dimerization along the rungs for $V_p = 2.8$, confirming a rung-dimerized band insulator (R-BI) phase. The phases at $\rho = 1/4$ and $3/4$ are related by particle-hole symmetry, so we present re-

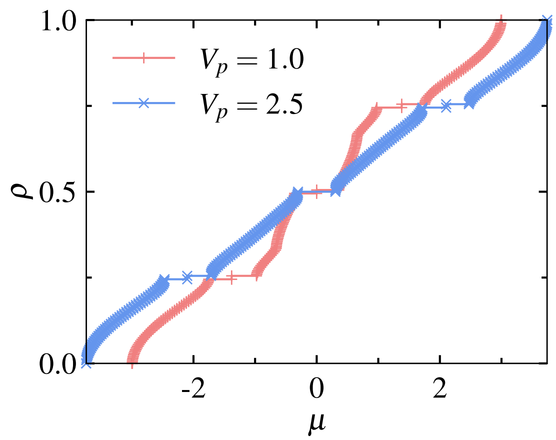

FIG. 10. The change in particle filling (ρ) as a function of change in chemical potential (μ) for different values of V_p for a system of $L = 100$ rungs keeping $t_1 = 0.2$, $t_2 = 1.0$, and $t_p = 0.8$ fixed. The plateaus at different filling ($\rho = 1/4$, $1/2$, and $3/4$) indicate the gap in the system and the length of the plateaus give an estimate of the gaps.

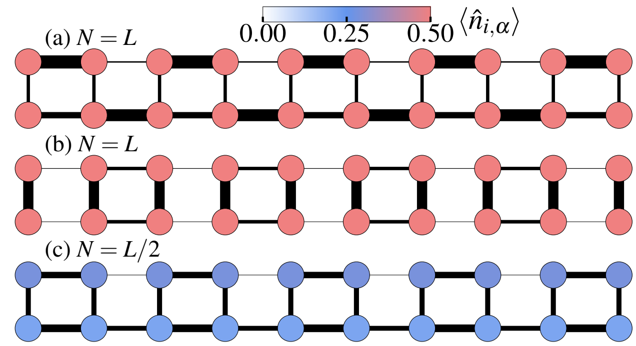

FIG. 11. The figure shows the magnitude of bond energies of all the bonds defined in Eq. (13) and the on-site particle density for different phases corresponding to Fig. 9 with a system consisting of $L = 100$ rungs keeping $t_1 = 0.2$, $t_2 = 1.0$, and $t_p = 0.8$ fixed. In the figures, the thickness of a bond is proportional to the respective magnitude of the bond energies, and the face color of the circles represents the values of $\langle \hat{n}_{i,\alpha} \rangle$. (a) The magnitude of bond energy and the onsite particle density at 1/2 filling ($N = L$) for $V_p = 0.2$, (b) $V_p = 2.8$, and (c) represents for 1/4 filling ($N = L/2$) at $V_p = 1.4$.

sults only for $\rho = 1/4$ corresponding to $V_p = 1.4$. In this case, a single particle is localized within alternate plaquettes and hop only within them, which we call a plaquette-ordered band insulator (PO-BI) phase.

Building on this understanding of the bulk phases, we now examine how the topological characteristics identified in the non-interacting limit evolve as a function of rung interaction. Note that the black dashed lines in Fig. 9 are the edge states, which also existed in the non-interacting limit (see Fig. 3). We obtain that these edge states also survive in the presence of interaction and at $\rho = 1/2$, with an increase in V_p, a gap-closing phase transition occurs to a trivial phase at $V_p \sim 2.3$, which we call the interaction-induced topological phase transition. To show that these states exist at the edges in the presence of finite interaction as well, we plot the on-site particle density of both the legs as a function of the rung index for $V_p = 0.2$ in Fig. 12(a). For comparison, we also show the onsite particle density $\langle \hat{n}_{i,\alpha} \rangle$corresponding to the trivial phase, i.e., at $V_p = 2.8$, which does not have any edge states as shown in Fig. 12(b). The clear asymmetry in density observed in both the edge sites for $V_p = 0.2$ confirms the edge states. In contrast, for $V_p = 2.8$, the density remains uniform throughout, confirming that there are no edge states in the system.

In order to quantify the topological nature of the system in the presence of interaction, we compute the Berry phase (γ) for a system of size $L = 12$ rungs using ED. The Berry phase γ, which is regarded as the topological invariant for the interacting system is computed using twisted boundary conditions. This involves modifying the hopping strength at the boundary as $t \to te^{i\theta}$, with θ being the twist angle [29, 96, 97]. As θ is varied from 0 to 2π, the many-body ground state $|\psi(\theta)\rangle$ acquires a geometric phase, known as the Berry phase (γ) [72], given by

$$\gamma = -\Im \ \ln \prod_{n=0}^{N_\theta - 1} \langle \psi_{\theta_n} | \psi_{\theta_{n+1}} \rangle. \tag{14}$$

where N_θ represents the number of discrete points between 0 to 2π. γ becomes 0 in the trivial phase and π in the topological phase. We compute the value of γ/π known as the winding number, and plot it as a function of V_p in Fig. 13 (a)(blue squares). The value of γ/π changes from 1 to 0 at $V_p \sim 2.3$, confirming the topological phase transition as a function of the interaction V_p.

The topological phases are often characterized by non-local string correlations [98–101], which can be captured by the string order parameter defined as

$$O_{\rm str}(r) = -\langle \hat{Z}_{\rm rung}(i) e^{i\frac{\pi}{2}\sum_{j=i+1}^{k-1} \hat{Z}_{\rm rung}(j)} \hat{Z}_{\rm rung}(k) \rangle, \tag{15}$$

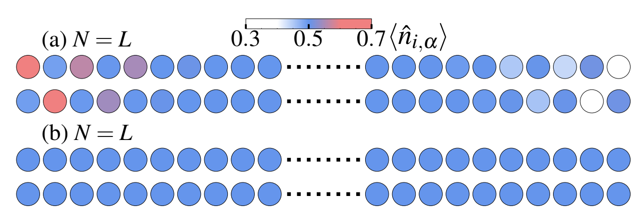

FIG. 12. On-site particle density for (a) $V_p = 0.2$ and (b) $V_p = 2.8$ keeping $t_1 = 0.2$, $t_2 = 1.0$, and $t_p = 0.8$ fixed. The face color of the circles represents the onsite particle density $\langle \hat{n}_{i,\alpha} \rangle$. To highlight the presence of edge states, only a few rungs near the boundary of a ladder with $L = 100$ rungs are displayed.

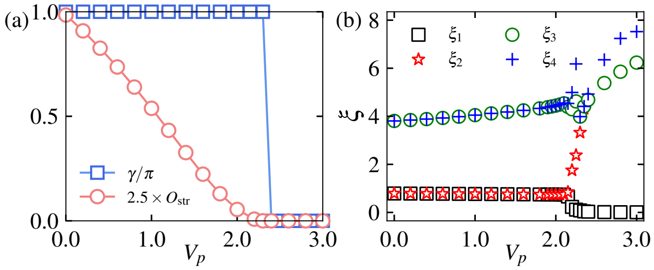

FIG. 13. (a) shows the winding number γ/π (squares) calculated using ED for a system of $L = 12$ rungs and the string order parameter $O_{\rm str}$ (circles) computed using DMRG for a system of $L = 100$ rungs as a function of V_p with the other parameters set to $t_1 = 0.2$, $t_2 = 1.0$, and $t_p = 0.8$. (b) shows the lowest four values of the entanglement spectrum (ξ_1, ξ_2, ξ_3, ξ_4) as a function of V_p, for a system of size $L = 200$ rungs.

where $\hat{Z}_{\rm rung}(i) = \hat{Z}_a(i) + \hat{Z}_b(i)$ and $\hat{Z}_\alpha(i) = 1 - 2\hat{\alpha}_i^\dagger\hat{\alpha}_i$. Here, i denotes the i^{th} rung of the ladder and $r = |i - k|$ represents the distance between the i^{th} and k^{th} rung. To avoid edge rungs, we have chosen $i = 2$ and $k = L - 1$. We compute $O_{\rm str}$ for a system of size $L = 100$ rungs and plot it along with the winding number in Fig. 13(a) (red circles). A comparison between the behavior of $O_{\rm str}$ and γ/π, reveals that $O_{\rm str}$ agrees well with the topological phase transition point identified from the winding number.

To further complement this topological phase transition, we compute the entanglement spectrum of the ground state, which serves as a powerful tool for detecting topological order, as it is related to the number of edge excitations in the system [32, 102–104]. The entanglement spectrum is obtained by logarithmically rescaling the eigenvalues of the reduced density matrix corresponding to a specific bipartition in the system. For a bipartition at l^{th} bond, the reduced density matrix is defined as $\rho_l = {\rm Tr}_{L-l}|\psi\rangle\langle\psi|$, where $|\psi\rangle$ is the ground state wave function. In the MPS representation used in DMRG, the squared singular values Λ_i^2 at bond l correspond to the eigenvalues λ_i of ρ_l. The entanglement spectrum is then given by

$$\xi_i \;=\; -\ln(\Lambda_i^2), \tag{16}$$

We compute the entanglement spectrum at the central bond of a system with $L = 200$ rungs and plot the four lowest levels ξ as a function of V_p in Fig. 13(b). A clear two-fold degeneracy appears in the range $0 \leq V_p \lesssim 2.3$, which is lifted outside this region. This degeneracy signals the presence of topological order in the ground state for $0 \leq V_p \lesssim 2.3$.

The above analysis demonstrates that the rung interaction (V_p) drives a topological phase transition, which in turn enables a Thouless charge pumping mechanism that is modulated by the rung interaction. Additionally, we also observe that the direction of charge pumping reverses for the opposite dimerization configuration in such an interacting system (not shown).

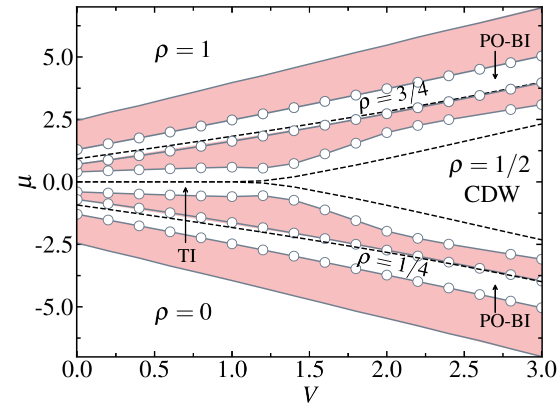

FIG. 14. The phase diagram in the $V - \mu$ plane keeping $t_1 = 0.2$, $t_2 = 1.0$, $t_p = 0.8$ fixed. Dashed lines represent the edge states. All the phase boundaries are extrapolated by taking a maximum system of size $L = 100$ rungs.

2. *Effect of uniform interaction*

For completeness, we also examine the case of uniform NN interactions applied equally along both the legs and the rungs, and analyze their effect on the topological phases present in the non-interacting limit.

The total Hamiltonian in this case is given by

$$\hat{H}_U = \hat{H} + \hat{H}_V \tag{17}$$

where $\hat{H}$ is the non-interacting part described earlier (Eq. (2)), and the interaction term $\hat{H}_V$ is defined as

$$\hat{H}_V = V\sum_i \left(\hat{n}_{i,a} - \frac{1}{2}\right)\left(\hat{n}_{i,b} - \frac{1}{2}\right) + V\sum_{i,\alpha}\left(\hat{n}_{i,\alpha} - \frac{1}{2}\right)\left(\hat{n}_{i+1,\alpha} - \frac{1}{2}\right) \tag{18}$$

To study the effect, we begin with a topological phase in the non-interacting limit by setting $t_1 = 0.2$, $t_2 = 1.0$, $t_p = 0.8$, and vary V. Figure 14 shows the resulting phase diagram in the V–μ plane. Three distinct gapped phases emerge at fillings $\rho = 1/4$, $1/2$, and $3/4$. However, unlike the case with only rung interactions, there is no gap-closing transition at $\rho = 1/2$. The zero-energy edge modes that exist at $V = 0$ (dashed lines) become energetic for $V \gtrsim 1.0$, indicating a transition between two gapped phases. To characterize the many-body phases at $\rho = 1/2$, we compute the NN bond energies and onsite particle densities as defined in Eq. (13) and depict their magnitude in Fig. 15(a) and (b) for two representative values of $V = 0.2$ and $V = 2.8$, respectively. At $V = 0.2$, the prominent oscillation in bond energy with

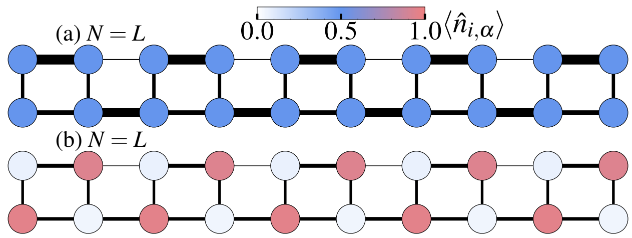

FIG. 15. The figure shows the magnitude of bond energies of all the bonds defined in Eq. (13) and the on-site particle density for different phases corresponding to Fig. 14 with a system consisting of $L = 100$ rungs keeping $t_1 = 0.2$, $t_2 = 1.0$, $t_p = 0.8$ fixed. Only the central 10 rungs of a system with $L = 100$ rungs are shown to focus on the bulk behavior. In the figures, the thickness of a bond is proportional to the respective magnitude of bond energy, and the face color of the circles represents the values of $\langle \hat{n}_{i,\alpha} \rangle$ for (a) $V = 0.2$, and (b) $V = 2.8$.

uniform particle densities indicate a BO phase. In contrast, for $V = 2.8$, the onsite density shows clear oscillations, signaling a charge-density wave (CDW) phase. Notably, this BO-to-CDW phase transition is not a standard topological phase transition, as it can be described by a local order parameter instead of a global topological invariant. Thus, we conclude that only rung interactions can drive a true topological phase transition in this system, whereas uniform interactions along both legs and rungs lead to a transition between gapped phases that can be described by local order parameters rather than global topological invariant.

IV. CONCLUSION

In this study, we have explored the effect of inter-leg coupling in establishing topological phases and phase transitions of spinless fermions on a two-leg ladder. By assuming that one of the legs possessing nearest-neighbour hopping dimerization and the other leg a uniform chain, we have shown that the entire ladder exhibits topological character irrespective of the dimerization pattern in the dimerized leg. As a result of this, we obtained two different topological phases of opposite character by changing the dimerization pattern of the leg possessing dimerized hopping. However, stronger inter-leg hopping makes the entire system a trivial insulator. Additionally, we showed that the inter-leg interactions can induce a distinct topological phase transition, revealing an interaction-induced topological phase transition in the system. We characterized these transitions by multiple diagnostics, including the entanglement spectrum, topological invariants, string order parameters and Thouless charge pumping.

Our study reveals topological phenomena involving spinless fermions on a quasi-1D geometry, which clearly highlights the intricate interplay between lattice geometry, many-body effects, and particle statistics in stabilizing the topological phase transitions in coupled systems. This also opens up possible avenues to explore the fate of these topological phases in bosonic and spinful fermionic many-body systems, in lattices other than ladder geometries, and in the presence of disorder.

V. ACKNOWLEDGMENT

We thank Sanchayan Banerjee for useful discussions. T.M. acknowledges support from Science and Engineering Research Board (SERB), Govt. of India, through project No. MTR/2022/000382 and STR/2022/000023.

VI. DATA AVAILABILITY

The data that support the findings of this article are openly available [105].

[1] Kenneth G. Wilson and J. Kogut, "The renormalization group and the ϵ expansion," Physics Reports **12**, 75–199 (1974).
[2] M. Z. Hasan and C. L. Kane, "Colloquium: Topological insulators," Rev. Mod. Phys. **82**, 3045–3067 (2010).
[3] W. P. Su, J. R. Schrieffer, and A. J. Heeger, "Solitons in polyacetylene," Phys. Rev. Lett. **42**, 1698–1701 (1979).
[4] János K. Asbóth, László Oroszlány, and András Pályi, "The su-schrieffer-heeger (ssh) model," in *A Short Course on Topological Insulators: Band Structure and Edge States in One and Two Dimensions* (Springer International Publishing, Cham, 2016) pp. 1–22.
[5] Adamantios Anastasiadis, Georgios Styliaris, Rajesh Chaunsali, Georgios Theocharis, and Fotios K. Diakonos, "Bulk-edge correspondence in the trimer su-schrieffer-heeger model," Phys. Rev. B **106**, 085109 (2022).
[6] Linhu Li, Zhihao Xu, and Shu Chen, "Topological phases of generalized su-schrieffer-heeger models," Phys. Rev. B **89**, 085111 (2014).
[7] Beatriz Pérez-González, Miguel Bello, Álvaro Gómez-León, and Gloria Platero, "Interplay between long-range hopping and disorder in topological systems," Phys. Rev. B **99**, 035146 (2019).
[8] N. Ahmadi, J. Abouie, and D. Baeriswyl, "Topological and nontopological features of generalized su-schrieffer-heeger models," Phys. Rev. B **101**, 195117 (2020).
[9] Marcos Atala, Monika Aidelsburger, Julio T. Barreiro, Dmitry Abanin, Takuya Kitagawa, Eugene Demler, and Immanuel Bloch, "Direct measurement of the zak

phase in topological bloch bands," Nature Physics **9**, 795 (2013).

[10] Shuta Nakajima, Takafumi Tomita, Shintaro Taie, Tomohiro Ichinose, Hideki Ozawa, Lei Wang, Matthias Troyer, and Yoshiro Takahashi, "Topological thouless pumping of ultracold fermions," Nature Physics **12**, 296 (2016).

[11] M. Lohse, C. Schweizer, O. Zilberberg, M. Aidelsburger, and I. Bloch, "A thouless quantum pump with ultracold bosonic atoms in an optical superlattice," Nature Physics **12**, 350–354 (2016).

[12] Sebabrata Mukherjee, Alexander Spracklen, Manuel Valiente, Erika Andersson, Patrik Öhberg, Nathan Goldman, and Robert R. Thomson, "Experimental observation of anomalous topological edge modes in a slowly driven photonic lattice," Nature Communications **8**, 13918 (2017).

[13] Ling Lu, John D. Joannopoulos, and Marin Soljačić, "Topological photonics," Nature Photonics **8**, 821–829 (2014).

[14] Luke Thatcher, Parker Fairfield, Lázaro Merlo-Ramírez, and Juan M Merlo, "Experimental observation of topological phase transitions in a mechanical 1d-ssh model," Physica Scripta **97**, 035702 (2022).

[15] Eric J. Meier, Fangzhao Alex An, and Bryce Gadway, "Observation of the topological soliton state in the su–schrieffer–heeger model," Nature Communications **7**, 13986 (2016).

[16] Dizhou Xie, Wei Gou, Teng Xiao, Bryce Gadway, and Bo Yan, "Topological characterizations of an extended su–schrieffer–heeger model," npj Quantum Information **5**, 55 (2019).

[17] Takuya Kitagawa, Matthew A. Broome, Alessandro Fedrizzi, Mark S. Rudner, Erez Berg, Ivan Kassal, Alán Aspuru-Guzik, Eugene Demler, and Andrew G. White, "Observation of topologically protected bound states in photonic quantum walks," Nature Communications **3**, 882 (2012).

[18] Martin Leder, Christopher Grossert, Lukas Sitta, Maximilian Genske, Achim Rosch, and Martin Weitz, "Real-space imaging of a topologically protected edge state with ultracold atoms in an amplitude-chirped optical lattice," Nature Communications **7**, 13112 (2016).

[19] Sylvain de Léséleuc, Vincent Lienhard, Pascal Scholl, Daniel Barredo, Sebastian Weber, Nicolai Lang, Hans Peter Büchler, Thierry Lahaye, and Antoine Browaeys, "Observation of a symmetry-protected topological phase of interacting bosons with rydberg atoms," Science **365**, 775–780 (2019).

[20] Nguyen H. Le, Andrew J. Fisher, Neil J. Curson, and Eran Ginossar, "Topological phases of a dimerized fermi–hubbard model for semiconductor nano-lattices," npj Quantum Information **6**, 24 (2020).

[21] Christina Jörg, Marius Jürgensen, Sebabrata Mukherjee, and Mikael C. Rechtsman, "Optical control of topological end states via soliton formation in a 1d lattice," Nanophotonics (2024), doi:10.1515/nanoph-2024-0401.

[22] Yu Liu, Yu-Ran Zhang, Yun-Hao Shi, Tao Liu, Congwei Lu, Yong-Yi Wang, Hao Li, Tian-Ming Li, Cheng-Lin Deng, Si-Yun Zhou, Tong Liu, Jia-Chi Zhang, Gui-Han Liang, Zheng-Yang Mei, Wei-Guo Ma, Hao-Tian Liu, Zheng-He Liu, Chi-Tong Chen, Kaixuan Huang, Xiaohui Song, S. P. Zhao, Ye Tian, Zhongcheng Xiang, Dongning Zheng, Franco Nori, Kai Xu, and Heng Fan, "Interplay between disorder and topology in thouless pumping on a superconducting quantum processor," Nature Communications **16**, 108 (2025).

[23] Xiaoling Wu, Xinhui Liang, Yaoqi Tian, Fan Yang, Cheng Chen, Yong-Chun Liu, Meng Khoon Tey, and Li You, "A concise review of rydberg atom based quantum computation and quantum simulation*," Chinese Physics B **30**, 020305 (2021).

[24] Yuqi Liu, Weidong Cao, Weijian Chen, Hua Wang, Lan Yang, and Xuan Zhang, "Fully integrated topological electronics," Scientific Reports **12**, 13410 (2022).

[25] Ching Hua Lee, Stefan Imhof, Christian Berger, Florian Bayer, Johannes Brehm, Laurens W. Molenkamp, Tobias Kiessling, and Ronny Thomale, "Topolectrical circuits," Communications Physics **1**, 39 (2018).

[26] Stephan Rachel, "Interacting topological insulators: a review," Reports on Progress in Physics **81**, 116501 (2018).

[27] Xie Chen, Zheng-Cheng Gu, and Xiao-Gang Wen, "Local unitary transformation, long-range quantum entanglement, wave function renormalization, and topological order," Phys. Rev. B **82**, 155138 (2010).

[28] T. Senthil, "Symmetry-protected topological phases of quantum matter," Annual Review of Condensed Matter Physics **6**, 299–324 (2015).

[29] Fabian Grusdt, Michael Höning, and Michael Fleischhauer, "Topological edge states in the one-dimensional superlattice bose-hubbard model," Phys. Rev. Lett. **110**, 260405 (2013).

[30] M. Di Liberto, A. Recati, I. Carusotto, and C. Menotti, "Two-body physics in the su-schrieffer-heeger model," Phys. Rev. A **94**, 062704 (2016).

[31] M. Di Liberto, A. Recati, I. Carusotto, and C. Menotti, "Two-body bound and edge states in the extended ssh bose-hubbard model," The European Physical Journal Special Topics **226**, 2751–2762 (2017).

[32] Xiaofan Zhou, Jian-Song Pan, and Suotang Jia, "Exploring interacting topological insulator in the extended su-schrieffer-heeger model," Phys. Rev. B **107**, 054105 (2023).

[33] Xiaopeng Li, Erhai Zhao, and W. Vincent Liu, "Topological states in a ladder-like optical lattice containing ultracold atoms in higher orbital bands," Nature Communications **4**, 1523 (2013).

[34] Luca Taddia, Eyal Cornfeld, Davide Rossini, Leonardo Mazza, Eran Sela, and Rosario Fazio, "Topological fractional pumping with alkaline-earth-like atoms in synthetic lattices," Phys. Rev. Lett. **118**, 230402 (2017).

[35] Joana Fraxanet, Daniel González-Cuadra, Tilman Pfau, Maciej Lewenstein, Tim Langen, and Luca Barbiero, "Topological quantum critical points in the extended bose-hubbard model," Phys. Rev. Lett. **128**, 043402 (2022).

[36] Sergi Julià-Farré, Javier Argüello-Luengo, Loïc Henriet, and Alexandre Dauphin, "Quantized thouless pumps protected by interactions in dimerized rydberg tweezer arrays," Phys. Rev. A **110**, 023328 (2024).

[37] Suman Mondal, Sebastian Greschner, Luis Santos, and Tapan Mishra, "Topological inheritance in two-component hubbard models with single-component su-schrieffer-heeger dimerization," Phys. Rev. A **104**, 013315 (2021).

[38] Pedro B. Melo, Sebastião A. S. Júnior, Wei Chen, Rubem Mondaini, and Thereza Paiva, "Topological marker approach to an interacting su-schrieffer-heeger model," Phys. Rev. B **108**, 195151 (2023).

[39] B. F. Márquez, N. Aucar Boidi, K. Hallberg, and A. A. Aligia, "Phase diagram and topology of the xxz chain with alternating bonds and staggered magnetic field," Phys. Rev. B **109**, 235143 (2024).

[40] Xiaofan Zhou, Suotang Jia, and Jian-Song Pan, "Interaction-induced phase transitions at topological quantum criticality of an extended su-schrieffer-heeger model," Phys. Rev. B **111**, 195117 (2025).

[41] Sepide Mohamadi and Jahanfar Abouie, "Emergence of topological non-fermi liquid phases in a modified su-schrieffer-heeger chain with long-range interactions," Phys. Rev. B **111**, 165129 (2025).

[42] Suman Mondal, Ashirbad Padhan, and Tapan Mishra, "Realizing a symmetry protected topological phase through dimerized interactions," Phys. Rev. B **106**, L201106 (2022).

[43] Balázs Hetényi, "Interaction-driven polarization shift in the $t{-}v{-}V^{'}$ lattice fermion model at half filling: Emergent haldane phase," Phys. Rev. Res. **2**, 023277 (2020).

[44] Sergi Julià-Farré, Daniel González-Cuadra, Alexander Patscheider, Manfred J. Mark, Francesca Ferlaino, Maciej Lewenstein, Luca Barbiero, and Alexandre Dauphin, "Revealing the topological nature of the bond order wave in a strongly correlated quantum system," Phys. Rev. Res. **4**, L032005 (2022).

[45] Zheng-Wei Zuo, Da-wei Kang, and Liben Li, New Journal of Physics **22**, 083057 (2020).

[46] Rajashri Parida, Diptiman Sen, and Tapan Mishra, "Topological phase transition through tunable nearest-neighbor interactions in a one-dimensional lattice," Phys. Rev. B **112**, 085124 (2025).

[47] Sergi Julià-Farré, Lorenzo Cardarelli, Maciej Lewenstein, Markus Müller, and Alexandre Dauphin, "Topological stripe state in an extended fermi-hubbard model," Phys. Rev. B **109**, 075109 (2024).

[48] A. A. Nersesyan, "Phase diagram of an interacting staggered su-schrieffer-heeger two-chain ladder close to a quantum critical point," Phys. Rev. B **102**, 045108 (2020).

[49] Shao-Liang Zhang and Qi Zhou, "Two-leg su-schrieffer-heeger chain with glide reflection symmetry," Phys. Rev. A **95**, 061601 (2017).

[50] C. Li, S. Lin, G. Zhang, and Z. Song, "Topological nodal points in two coupled su-schrieffer-heeger chains," Phys. Rev. B **96**, 125418 (2017).

[51] Karmela Padavić, Suraj S. Hegde, Wade DeGottardi, and Smitha Vishveshwara, "Topological phases, edge modes, and the hofstadter butterfly in coupled su-schrieffer-heeger systems," Phys. Rev. B **98**, 024205 (2018).

[52] Ashirbad Padhan, Suman Mondal, Smitha Vishveshwara, and Tapan Mishra, "Interacting bosons on a su-schrieffer-heeger ladder: Topological phases and thouless pumping," Phys. Rev. B **109**, 085120 (2024).

[53] Suman Mondal, Adhip Agarwala, Tapan Mishra, and Abhishodh Prakash, "Symmetry-enriched criticality in a coupled spin ladder," Phys. Rev. B **108**, 245135 (2023).

[54] Chunhan Feng, Bo Xing, Dario Poletti, Richard Scalettar, and George Batrouni, "Phase diagram of the su-schrieffer-heeger-hubbard model on a square lattice," Phys. Rev. B **106**, L081114 (2022).

[55] Rajashri Parida, Ashirbad Padhan, and Tapan Mishra, "Interaction driven topological phase transitions of hardcore bosons on a two-leg ladder," Phys. Rev. B **110**, 165110 (2024).

[56] C A Downing, L Martín-Moreno, and O I R Fox, "Unconventional edge states in a two-leg ladder," New Journal of Physics **26**, 073014 (2024).

[57] Takuhiro Ogino, Shunsuke Furukawa, Ryui Kaneko, Satoshi Morita, and Naoki Kawashima, "Symmetry-protected topological phases and competing orders in a spin-$\frac{1}{2}$ xxz ladder with a four-spin interaction," Phys. Rev. B **104**, 075135 (2021).

[58] Takuhiro Ogino, Ryui Kaneko, Satoshi Morita, and Shunsuke Furukawa, "Ground-state phase diagram of a spin-$\frac{1}{2}$ frustrated xxz ladder," Phys. Rev. B **106**, 155106 (2022).

[59] Zheng-Xin Liu, Zhen-Biao Yang, Yong-Jian Han, Wei Yi, and Xiao-Gang Wen, "Symmetry-protected topological phases in spin ladders with two-body interactions," Phys. Rev. B **86**, 195122 (2012).

[60] Sara Aghtouman and Mir Vahid Hosseini, "Dimerized hofstadter model in two-leg ladder quasi-crystals," Scientific Reports **14**, 8782 (2024).

[61] João Pedro Gama D'Elia and Thereza Paiva, "Topological phase transition in the two-leg hubbard model: Emergence of the haldane phase via diagonal hopping and strong interactions," Phys. Rev. B **112**, 035169 (2025).

[62] Milad Jangjan and Mir Vahid Hosseini, "Floquet engineering of topological metal states and hybridization of edge states with bulk states in dimerized two-leg ladders," Scientific Reports **10**, 14256 (2020).

[63] Milad Jangjan and Mir Vahid Hosseini, "Topological properties of subsystem-symmetry-protected edge states in an extended quasi-one-dimensional dimerized lattice," Phys. Rev. B **106**, 205111 (2022).

[64] Jie Lu and Shidong Wang, "Tight-binding investigation of the metallic proximity effect of semiconductor-metal double-wall carbon nanotubes," Phys. Rev. B **76**, 233103 (2007).

[65] T. Shoman, A. Takayama, T. Sato, S. Souma, T. Takahashi, T. Oguchi, Kouji Segawa, and Yoichi Ando, "Topological proximity effect in a topological insulator hybrid," Nature Communications **6**, 6547 (2015).

[66] Timothy H. Hsieh, Hiroaki Ishizuka, Leon Balents, and Taylor L. Hughes, "Bulk topological proximity effect," Phys. Rev. Lett. **116**, 086802 (2016).

[67] Peng Cheng, Philipp W. Klein, Kirill Plekhanov, Klaus Sengstock, Monika Aidelsburger, Christof Weitenberg, and Karyn Le Hur, "Topological proximity effects in a haldane graphene bilayer system," Phys. Rev. B **100**, 081107 (2019).

[68] Jun-Hui Zheng and Walter Hofstetter, "Topological invariant for two-dimensional open systems," Phys. Rev. B **97**, 195434 (2018).

[69] J. Ignacio Cirac, David Pérez-García, Norbert Schuch, and Frank Verstraete, "Matrix product states and projected entangled pair states: Concepts, symmetries, theorems," Rev. Mod. Phys. **93**, 045003 (2021).

[70] Ulrich Schollwöck, "The density-matrix renormalization group in the age of matrix product states," Annals of Physics **326**, 96–192 (2011), january 2011 Special Issue.

[71] Fran çois Crépin, Nicolas Laflorencie, Guillaume Roux, and Pascal Simon, "Phase diagram of hard-core bosons on clean and disordered two-leg ladders: Mott insulator–luttinger liquid–bose glass," Phys. Rev. B **84**, 054517 (2011).

[72] Michael Victor Berry, "Quantal phase factors accompanying adiabatic changes," Proc. Roy. Soc. London **A 392**, 45–57 (1984).

[73] D. J. Thouless, "Quantization of particle transport," Phys. Rev. B **27**, 6083–6087 (1983).

[74] Roberta Citro and Monika Aidelsburger, "Thouless pumping and topology," Nature Reviews Physics **5**, 87–101 (2023).

[75] A. Hayward, C. Schweizer, M. Lohse, M. Aidelsburger, and F. Heidrich-Meisner, "Topological charge pumping in the interacting bosonic rice-mele model," Phys. Rev. B **98**, 245148 (2018).

[76] M. J. Rice and E. J. Mele, "Elementary excitations of a linearly conjugated diatomic polymer," Phys. Rev. Lett. **49**, 1455–1459 (1982).

[77] János K. Asbóth, László Oroszlány, and András Pályi, "Adiabatic charge pumping, rice-mele model," in *A Short Course on Topological Insulators: Band Structure and Edge States in One and Two Dimensions* (Springer International Publishing, Cham, 2016) pp. 55–68.

[78] Ling Lin, Yongguan Ke, and Chaohong Lee, "Interaction-induced topological bound states and thouless pumping in a one-dimensional optical lattice," Phys. Rev. A **101**, 023620 (2020).

[79] Yongguan Ke, Xizhou Qin, Yuri S. Kivshar, and Chaohong Lee, "Multiparticle wannier states and thouless pumping of interacting bosons," Phys. Rev. A **95**, 063630 (2017).

[80] Javier Argüello-Luengo, Manfred J. Mark, Francesca Ferlaino, Maciej Lewenstein, Luca Barbiero, and Sergi Julià-Farré, "Stabilization of Hubbard-Thouless pumps through nonlocal fermionic repulsion," Quantum **8**, 1285 (2024).

[81] Yoshihito Kuno, Keita Shimizu, and Ikuo Ichinose, "Various topological mott insulators and topological bulk charge pumping in strongly-interacting boson system in one-dimensional superlattice," New Journal of Physics **19**, 123025 (2017).

[82] E. Bertok, F. Heidrich-Meisner, and A. A. Aligia, "Splitting of topological charge pumping in an interacting two-component fermionic rice-mele hubbard model," Phys. Rev. B **106**, 045141 (2022).

[83] Suman Mondal, Eric Bertok, and Fabian Heidrich-Meisner, "Phonon-induced breakdown of thouless pumping in the rice-mele-holstein model," Phys. Rev. B **106**, 235118 (2022).

[84] C. Schweizer, M. Lohse, R. Citro, and I. Bloch, "Spin pumping and measurement of spin currents in optical superlattices," Phys. Rev. Lett. **117**, 170405 (2016).

[85] Yaacov E. Kraus, Yoav Lahini, Zohar Ringel, Mor Verbin, and Oded Zilberberg, "Topological states and adiabatic pumping in quasicrystals," Phys. Rev. Lett. **109**, 106402 (2012).

[86] Lei Wang, Matthias Troyer, and Xi Dai, "Topological charge pumping in a one-dimensional optical lattice," Phys. Rev. Lett. **111**, 026802 (2013).

[87] Anne-Sophie Walter, Zijie Zhu, Marius Gächter, Joaquín Minguzzi, Stephan Roschinski, Kilian Sandholzer, Konrad Viebahn, and Tilman Esslinger, "Quantization and its breakdown in a hubbard–thouless pump," Nature Physics **19**, 1471–1475 (2023).

[88] Yongguan Ke, Janet Zhong, Alexander V. Poshakinskiy, Yuri S. Kivshar, Alexander N. Poddubny, and Chaohong Lee, "Radiative topological biphoton states in modulated qubit arrays," Phys. Rev. Res. **2**, 033190 (2020).

[89] Marius Jürgensen, Sebabrata Mukherjee, Christina Jörg, and Mikael C. Rechtsman, "Quantized fractional thouless pumping of solitons," Nature Physics **19**, 420–426 (2023).

[90] Marius Jürgensen, Sebabrata Mukherjee, and Mikael C. Rechtsman, "Quantized nonlinear thouless pumping," Nature **596**, 63–67 (2021).

[91] Konrad Viebahn, Anne-Sophie Walter, Eric Bertok, Zijie Zhu, Marius Gächter, Armando A. Aligia, Fabian Heidrich-Meisner, and Tilman Esslinger, "Interactions enable thouless pumping in a nonsliding lattice," Phys. Rev. X **14**, 021049 (2024).

[92] Zijie Zhu, Marius Gächter, Anne-Sophie Walter, Konrad Viebahn, and Tilman Esslinger, "Reversal of quantized hall drifts at noninteracting and interacting topological boundaries," Science **384**, 317–320 (2024).

[93] Toshiya Hikihara, Lars Kecke, Tsutomu Momoi, and Akira Furusaki, "Vector chiral and multipolar orders in the spin-$\frac{1}{2}$ frustrated ferromagnetic chain in magnetic field," Phys. Rev. B **78**, 144404 (2008).

[94] Tapan Mishra, Sebastian Greschner, and Luis Santos, "Frustration-induced supersolids in the absence of intersite interactions," Phys. Rev. B **92**, 195149 (2015).

[95] Tapan Mishra, Sebastian Greschner, and Luis Santos, "Polar molecules in frustrated triangular ladders," Phys. Rev. A **91**, 043614 (2015).

[96] J. Zak, "Berry's phase for energy bands in solids," Phys. Rev. Lett. **62**, 2747–2750 (1989).

[97] R. Resta and S. Sorella, "Many-body effects on polarization and dynamical charges in a partly covalent polar insulator," Phys. Rev. Lett. **74**, 4738–4741 (1995).

[98] Marcel den Nijs and Koos Rommelse, "Preroughening transitions in crystal surfaces and valence-bond phases in quantum spin chains," Phys. Rev. B **40**, 4709–4734 (1989).

[99] Hal Tasaki, "Quantum liquid in antiferromagnetic chains: A stochastic geometric approach to the haldane gap," Phys. Rev. Lett. **66**, 798–801 (1991).

[100] Kazuo Hida, "Crossover between the haldane-gap phase and the dimer phase in the spin-1/2 alternating heisenberg chain," Phys. Rev. B **45**, 2207–2212 (1992).

[101] Sandra J. Gibson, R. Meyer, and Gennady Y. Chitov, "Numerical study of critical properties and hidden orders in dimerized spin ladders," Phys. Rev. B **83**, 104423 (2011).

[102] Hui Li and F. D. M. Haldane, "Entanglement spectrum as a generalization of entanglement entropy: Identification of topological order in non-abelian fractional quantum hall effect states," Phys. Rev. Lett. **101**, 010504 (2008).

[103] Tsuneya Yoshida, Robert Peters, Satoshi Fujimoto, and Norio Kawakami, "Characterization of a topological mott insulator in one dimension," Phys. Rev. Lett. **112**, 196404 (2014).

[104] Ari M. Turner, Frank Pollmann, and Erez Berg, "Topological phases of one-dimensional fermions: An entanglement point of view," Phys. Rev. B **83**, 075102 (2011).

[105] Rajashri Parida, Biswajit Paul, Soumya Ranjan Padhi, and Tapan Mishra, "Coupling induced emergent topology in a two-leg fermionic ladder," 10.5281/zenodo.17279150.